ADVANCED MATERIALS
www.advmat.de

Open-Shell Nanosensitizers for Glutathione Responsive Cancer Sonodynamic Therapy

Han Wang, Jinxiao Guo, Wilson Lin, Zi Fu, Xiuru Ji, Bo Yu, Min Lu, Wenguo Cui, Lianfu Deng, Jonathan W. Engle, Zhiyuan Wu, Weibo Cai,* and Dalong Ni**

Deleterious effects to normal tissues and short biological half-life of sonosensitizers limit the applications of sonodynamic therapy (SDT). Herein, a new sonosensitizer (Cu(II)NS) is synthesized that consists of porphyrins, chelated Cu^{2+}, and poly(ethylene glycol) (PEG) to overcome the challenges of SDT. As Cu^{2+} contains 27 electrons, Cu(II)NS has an unpaired electron (open shell), resulting in a doublet ground state and little sonosensitivity. Overexpressed glutathione in the tumor can reduce Cu^{2+} to generate Cu(I)NS, leading to a singlet ground state and recuperative sonosensitivity. Additionally, PEG endows Cu(II)NS with increased blood biological half-life and enhanced tumor accumulation, further increasing the effect of SDT. Through regulating the valence state of Cu, cancer SDT with enhanced therapeutic index is achieved.

1. Introduction

In the past decade, sonodynamic therapy (SDT) has received much attention because of its favorable penetration depth in biological tissues and noninvasive therapeutic procedure.[1] Generally, upon excitation of sonoluminescence, sonosensitizers convert triplet oxygen ($^3O_2$) or H_2O to reactive oxygen species (ROS), which can destroy cancer cells effectively.[2] Recently, several sonosensitizers such as porphyrins, TiO_2, Bi_2MoO_6, and $BaTiO_3$ have been developed and yield impressive therapeutic effects.[1] Nevertheless, there are still several obstacles that impede applications of SDT. SDT damages healthy tissues surrounding the tumor, and the phototoxicity of sonosensitizers to skin cannot be ignored.[2] Additionally, the majority of sonosensitizers have a short blood half-life period, which will induce insufficient tumor accumulation and lead to unfavorable curative effects.[2] Hence, it is highly important to develop sonosensitizers with less side-effect and longer circulation period simultaneously.

With the development of nanomedicine, tumor microenvironment (TME) responsive nanomaterials have the potential to address several of the issues discussed above.[3] It is widely known that TME contains overexpressed H^+, glutathione (GSH), matrix metalloproteinase, etc.[4] Our group has used these excess molecules to regulate the valence states of certain atoms in nanomaterials that result in more precise treatment. We reported that the hexavalent Mo atoms of molybdophosphate-based nanomaterials could react with GSH in tumor to achieve better photothermal performance.[5] The change of valence states such as Cu(II)/Cu(I), Mo(VI)/Mo(V), Ti(IV)/Ti(III), and Pt(IV)/Pt(II) can usually bring changes in physicochemical properties including catalysis, magnetism, energy band structure, and toxicity.[6] Hence, TME-triggered valence change has potential to assist sonosensitizers to achieve more accurate SDT.

Recently, our group synthesized a series of porphyrin–poly(ethylene glycol) (PEG)-based nanoprobe for cancer multimodal imaging.[7] The introduction of PEG increases nanoprobes' circulation time, and porphyrin acts as the SDT agent. Herein we report a nanosensitizer (Cu(II)NS) containing tetrakis carboxyphenyl porphyrin (TCPP), TCPP-chelated Cu^{2+}, and 8-arm-PEG-NH_2 for more precise and effective SDT (**Figure 1a**). Generally, organic sonosensitizers usually have

H. Wang, Z. Fu, X. Ji, M. Lu, W. Cui, L. Deng, D. Ni
Department of Orthopaedics
Shanghai Key Laboratory for Prevention and Treatment of Bone and Joint Diseases
Shanghai Institute of Traumatology and Orthopaedics
Ruijin Hospital
Shanghai Jiao Tong University School of Medicine
Shanghai 200025, P. R. China
E-mail: ndl12353@rjh.com.cn

J. Guo
Department of Orthopaedics
Shanghai Jiao Tong University Affiliated Sixth People's Hospital
Shanghai Jiao Tong University
Shanghai 200233, P. R. China

W. Lin, B. Yu, J. W. Engle, W. Cai
Departments of Radiology and Medical Physics
University of Wisconsin
Madison, WI 53705, USA
E-mail: wcai@uwhealth.org

Z. Wu
Department of Interventional Radiology
Ruijin Hospital
Shanghai Jiao Tong University School of Medicine
Shanghai 200025, P. R. China
E-mail: wuzhiyuan@shsmu.edu.cn

The ORCID identification number(s) for the author(s) of this article can be found under https://doi.org/10.1002/adma.202110283.

DOI: 10.1002/adma.202110283

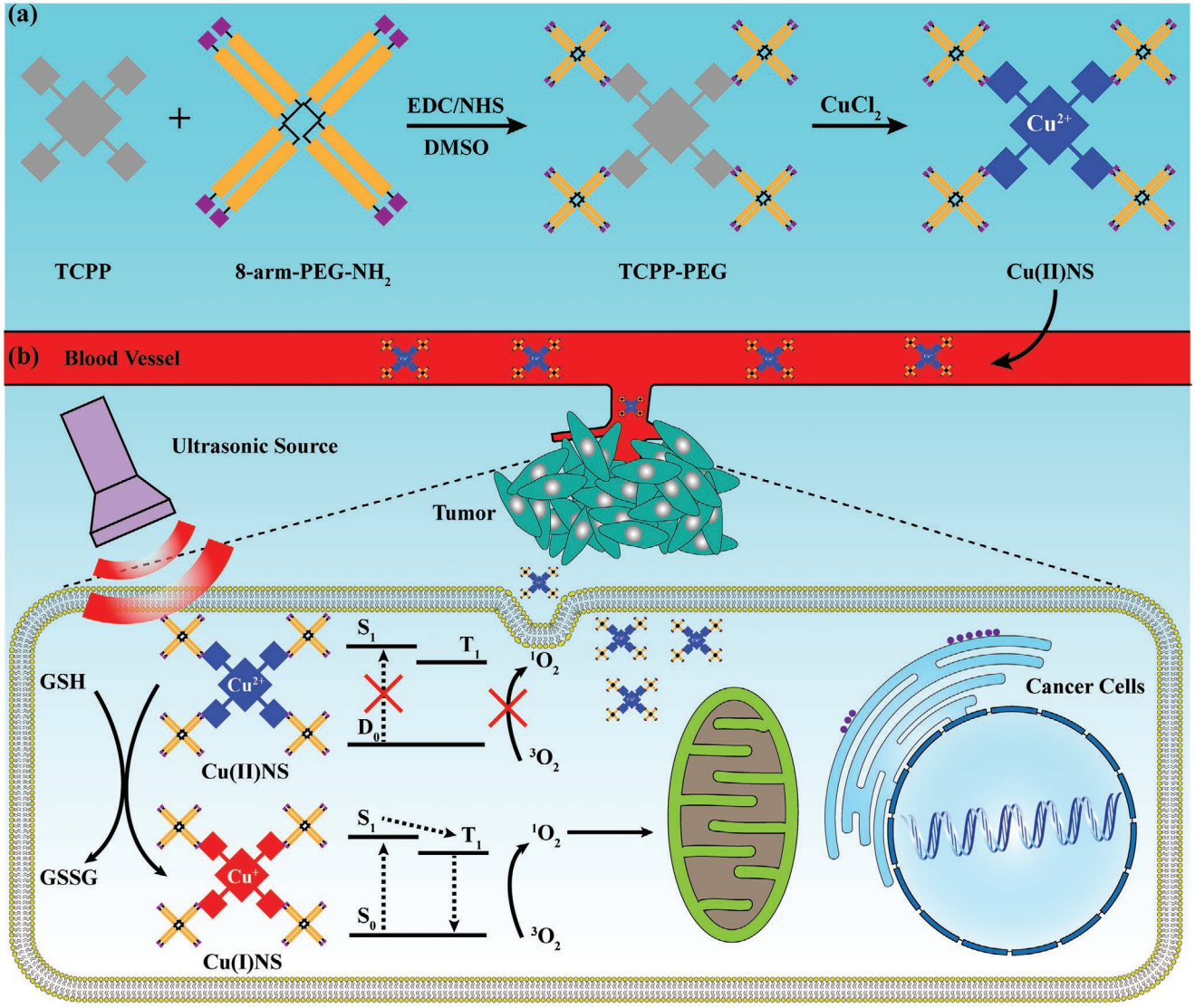

Figure 1. a) Synthetic procedure of Cu(II)NS. b) Illustration of open-shell Cu(II)NS for GSH-responsive sonodynamic therapy (SDT).

a closed-shell structure, which means all the electrons are paired and the ground state is singlet (S_0). As seen from the Jablonski diagram, sonoluminescence excites S_0 to S_1 state, then, through intersystem crossing (ISC), S_1 transitions to the triplet state (T_1).[8] T_1 can convert triplet oxygen ($^3O_2$) to singlet oxygen ($^1O_2$) and relax to S_0 in the process.[9] As a single Cu^{2+} has 27 electrons, there is an unpaired electron in Cu-TCPP complex, inducing that Cu(II)NS is open-shell and the ground state is doublet (D_0). Consequently, Cu(II)NS cannot produce ROS upon sonication in normal tissues. When Cu(II)NS enter into tumors, the overexpressed GSH reduces Cu(II)NS (Cu^{2+}) to Cu(I)NS (Cu^+). As Cu^+ has 28 electrons, there are no unpaired electrons. Hence Cu(I)NS is closed-shell and can produce $^1O_2$ in SDT (Figure 1b). Through GSH-regulated valence change of Cu(II)/Cu(I), Cu(II)NS can achieve more accurate SDT. In addition, due to the long circulation period of porphyrin–PEG, the high tumor accumulation of nanosensitizers will further enhance the effect of SDT.[7a,b] We believe that the strategy of regulating valence state not only increases the therapeutic index of SDT, but also spurs more ideas for the design of nanomaterials.

2. Nanomaterial Synthesis and Characterization

The synthetic procedure of Cu(II)NS is presented in Figure 1a. The TCPP and 8-arm-PEG-NH_2 were used to synthesize TCPP-PEG nanoparticles. Then, Cu^{2+} was chelated by TCPP-PEG to yield Cu(II)NS. For observing the chelation rate, in consideration of the emitted positron and almost the same chemical properties, $^{64}Cu^{2+}$ instead of Cu^{2+} was used, which can easily be detected by positron emission tomography (PET). From the radiochromatograph shown in Figure S1a–c, Supporting Information, we find that the increase of the reaction time and temperature leads to an increasing yield of ^{64}Cu(II)NS. When the reaction time is 2 h and the temperature is 70 °C, the yield can reach almost 100% (Figure S2, Supporting Information). Interestingly, as shown in Figure S3, Supporting Information, the

chelation rate is inversely proportional to fluorescence intensity, which means Cu(II)NS have little fluorescence. Even if we prolong the reaction time, the yield of ^{64}Cu(II)NS changes a little (Figure S4, Supporting Information). Ultraviolet–visible spectrum of TCPP-PEG shows that there are four peaks from 500 to 700 nm, due to the nonequivalent N atoms in the porphyrin ring of TCPP. While after chelation there is only one peak (Figure S5, Supporting Information) due to the increase of spatial symmetry (the coordination between four N atoms and Cu^{2+}).[10]

Then we characterize the differences between Cu(II)NS and Cu(I)NS. Cu(I)NS was obtained through the reaction between Cu(II)NS and GSH. Briefly, Cu(II)NS solution (10×10^{-3} M, 1 mL) and GSH solution (10×10^{-3} M, 2 mL) were mixed and shocked at 37 °C for 120 min. Transmission electron microscopy (TEM) image shows that the size of Cu(II)NS is about 20 nm (**Figure 2**a). The size and the morphology of as-prepared Cu(I)NS is similar to that of Cu(II)NS (Figure 2b and Figure S6, Supporting Information). The result of dynamic light scattering measurements agrees with TEM (Figure 2b), indicating that there are few morphological changes between Cu(II)NS and Cu(I)NS. X-ray photoelectron spectroscopy (XPS) of Cu 2p shows that the ratio of Cu(II)/Cu(I) in Cu(II)NS is 0.675 (Figure 2c,d). The existence of Cu(I) in Cu(II)NS can be due to the coordination bond of Cu—N. While the ratio of Cu(II)/Cu(I) is 0.254 in the obtained Cu(I)NS (Figure 2c,e), indicating that GSH could reduce Cu(II) to Cu(I).

As discussed above, Cu(II)NS have unpaired electrons while Cu(I)NS do not. This was verified by measuring the hysteresis loop of Cu(I)NS and Cu(II)NS. As presented in Figure 2f, Cu(II)NS exhibit obvious paramagnetism while Cu(I)NS show diamagnetism, in accordance with the preconceived electron structure. In addition, the fluorescence emission peak and fluorescence lifetime of Cu(I)NS is similar to TCPP-PEG, but little fluorescence can be detected in Cu(II)NS (Figure 2g,h and Figure S7a,b, Supporting Information), in accordance with the data in Figure S3, Supporting Information. As fluorescence comes from the transition from S_n ($n \geq 1$) to S_0, these data

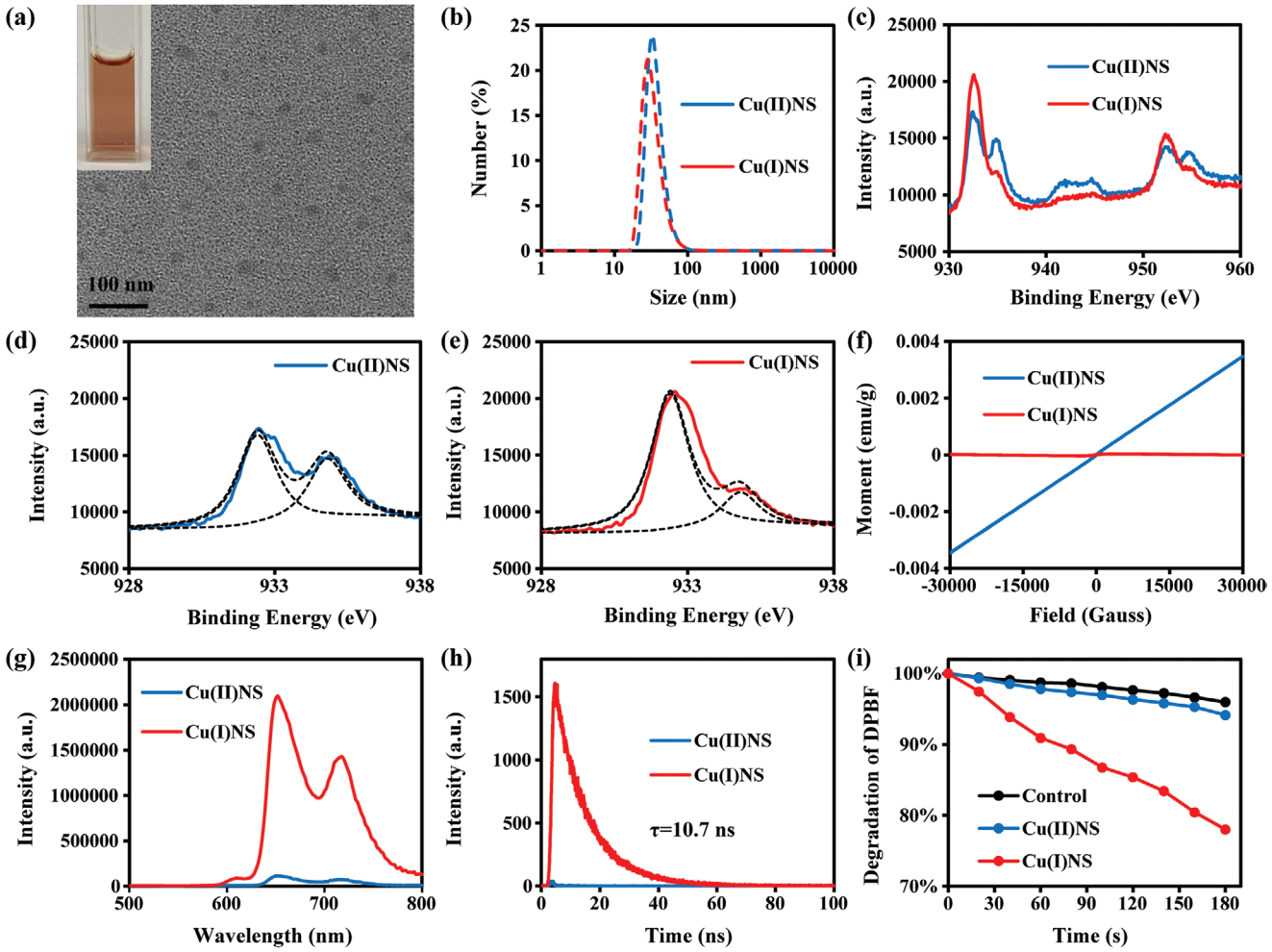

Figure 2. Characterization of Cu(II)NS. a) TEM image of Cu(II)NS (insert: photograph of Cu(II)NS solution). b) Hydrodynamic size of Cu(II)NS and Cu(I)NS. c) XPS spectra (Cu 2p) of Cu(II)NS and Cu(I)NS. d,e) XPS peak fitting of Cu(II)NS (d) and of Cu(I)NS (e). f) Hysteresis loop of Cu(II)NS and Cu(I)NS. g) Fluorescence spectrum of Cu(II)NS and Cu(I)NS (excitation wavelength: 300 nm). h) Fluorescence lifetime (650 nm) of Cu(II)NS and Cu(I)NS (excitation wavelength: 300 nm). i) The yield of singlet oxygen of deionized water (control group), Cu(II)NS, and Cu(I)NS upon excitation of ultrasound (1 MHz, 50% duty cycle, 1 W cm^{-2}) measured by the degradation of 1,3-diphenylisobenzofuran (DPBF).

indicate that the ground state of Cu(I)NS is S_0 but the ground state of Cu(II)NS is not. Finally, the yield of $^1O_2$ in solution was detected after sonication. Based on our earlier discussions, it is not surprising that after treated by ultrasound (US) for 180 s, Cu(I)NS produces 3.8 times and 5.5 times of $^1O_2$ (measured by the degradation of 1,3-diphenylisobenzofuran) higher than that of Cu(II)NS and the control, respectively (Figure 2i).

To further explain the data, the excited state of Cu(II)NS and Cu(I)NS were calculated. Simulated calculation was performed based on density functional theory (DFT) by using B3LYP/6-31G(d,p).[11] The excitation energy was calculated via the time-dependent DFT method. All the calculations take the solvation effect of water into consideration via the polarizable continuum model method. The model structures were optimized until the max force below 0.000450 Ha Bohr^{-1}. As shown in **Figure** 3a, we find that compared to Cu(II)NS, Cu(I)NS own higher symmetry and less distortion. In addition, Cu(I)NS have more allowable excited state levels and higher oscillator strength (Figure 3b), which can provide more opportunities for the transition of electrons. Generally, the conversion process of US to $^1O_2$ includes sonoluminescence, electron excitation (S_0–S_1), ISC (S_1–T_1), and interaction between T_1 and $^3O_2$ (Figure 3c). Fluorescence spectrum indicates that Cu(II)NS have little electron excitation. Hysteresis loop shows that Cu(II)NS have no S_0 state. Simulated calculation further shows that Cu(II)NS have few allowable excited state levels. As concluded in Figure 3c, D_0 and D_1 state of Cu(II)NS can hardly jump to S_1 and T_1 (forbidden transition), respectively. As mentioned above that GSH could convert Cu(II)NS to Cu(I)NS, thus, our calculations and results in solution indicate that GSH-triggered SDT is feasible.

3. In Vitro and In Vivo Investigations

Encouraged by the results in solution, we investigated the performance of Cu(II)NS and Cu(I)NS in vitro on 4T1 cells. As shown by cellular uptake of Cu(II)NS in **Figure** 4a, red fluorescence gradually become brighter as time goes on, due to the uptake of Cu(II)NS and the reduction by intracellular GSH. It is worth mentioning that sonosensitizer can stay in cells for more than 12 h (Figure 4a). The content of oxidized glutathione (GSSG) also increases along with the uptake of Cu(II)NS (Figure 4b), further indicating the reaction between Cu(II)NS and GSH. The yield of $^1O_2$ in cells was evaluated. As shown in Figure 4c,d, measured by DCFH-DA (intracellular ROS probe) and singlet oxygen sensor green (SOSG), Cu(II)NS+US can generate much more $^1O_2$ than just US. Consequently, Cu(II)NS+US resulted in inducing the most cell apoptosis, meanwhile control group, US-only group, and Cu(II)NS-only group induced few cell apoptosis (Figure 4e). In accordance with previous studies, the US alone (1 MHz, 1 W cm^{-2}) showed few damages to cancer cells.[12] In addition, cell viability measured by CCK-8 assay showed similar results. As presented in Figure 4f, the viability of sonicated cells decreased along with the increase of the concentration of Cu(II)NS. When treated with 10 μM Cu(II)NS, the viability of sonicated cells was only 23%, while the viability of cells without US treating was still 95%.

Having proved the effect of GSH-triggered SDT in vitro, the performance of Cu(II)NS in vivo based on 4T1-tumor-bearing mice was examined. PET imaging was used to measure the image-derived biodistribution of Cu(II)NS in vivo. As shown from the PET maximum intensity projection images in

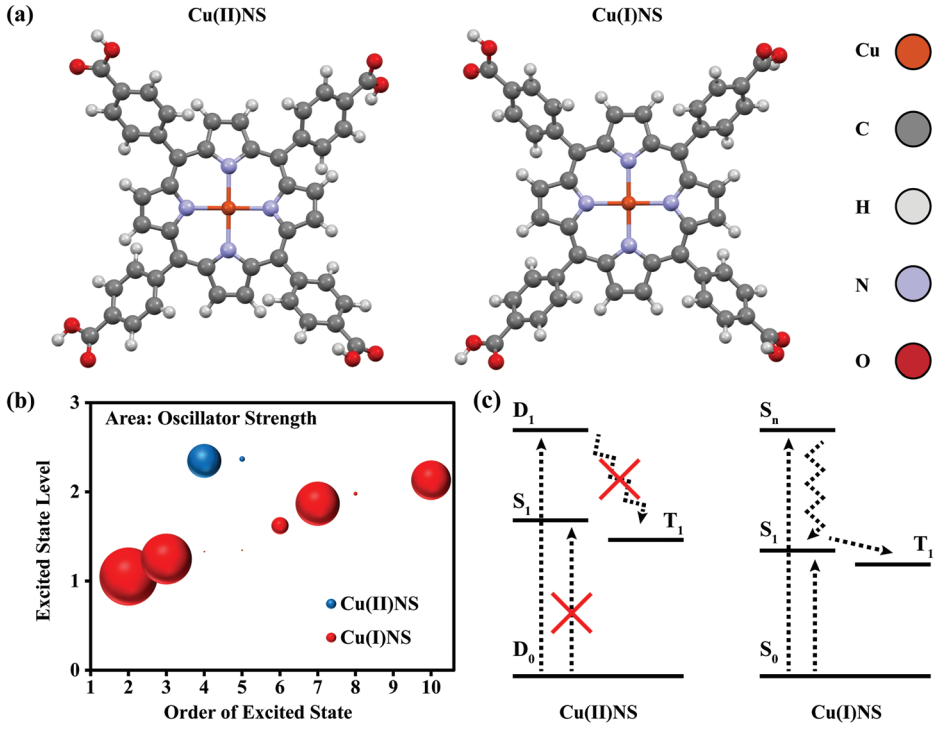

Figure 3. a) Simulated conformation of Cu(II)NS and Cu(I)NS. b) Calculated excited state level and oscillator strength of Cu(II)NS and Cu(I)NS. c) The mechanism of GSH-triggered SDT.

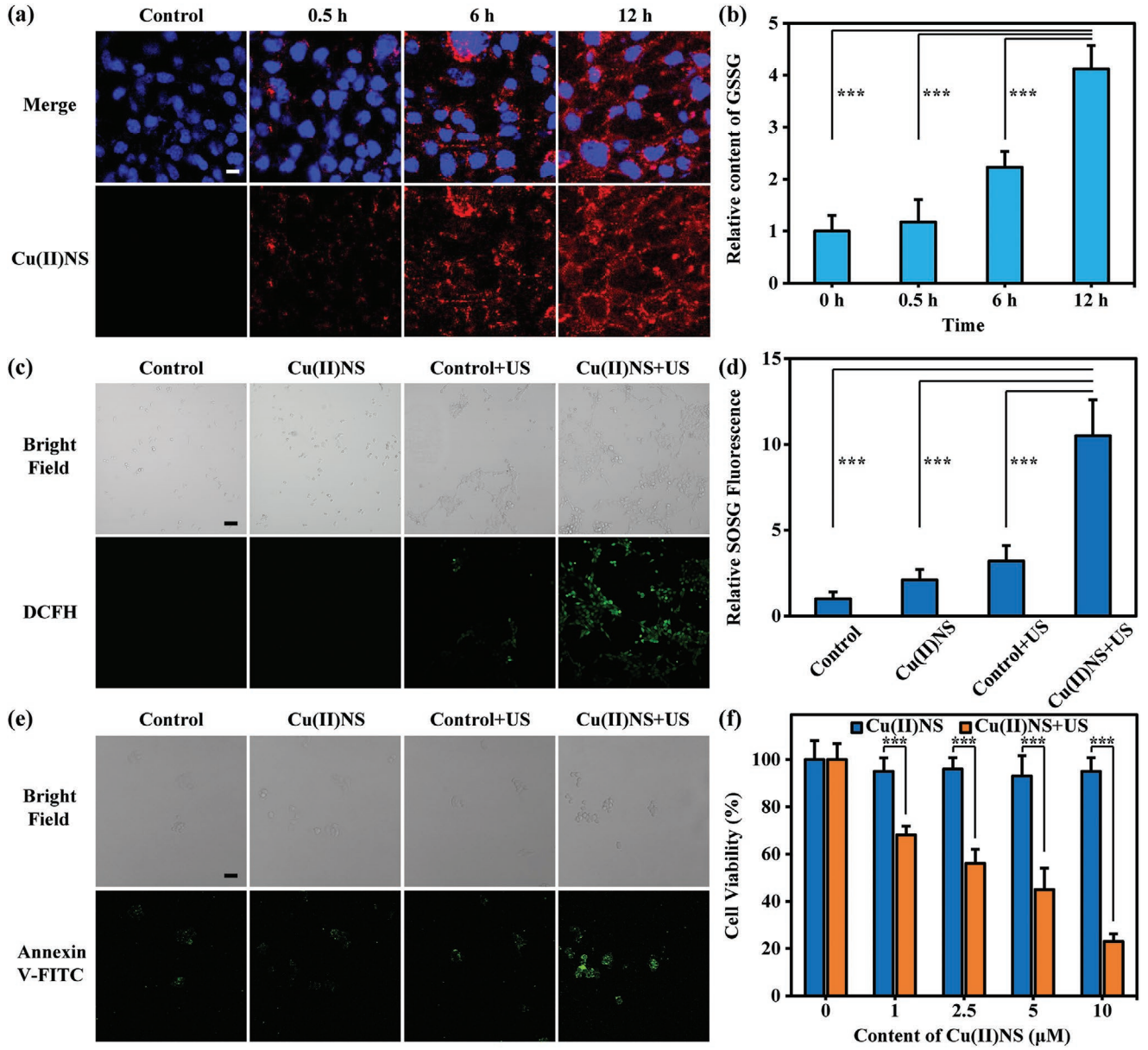

Figure 4. In vitro experiments by using 4T1 cells. a) Cytophagy of Cu(II)NS measured by confocal laser scanning microscopy (CLSM). b) Relative content of oxidized glutathione (GSSG) after the addition of Cu(II)NS (n = 5, mean ± SD). c) The yield of ROS of each group measured by DCFH. d) The yield of singlet oxygen measured by SOSG (n = 5, mean ± SD). e) The apoptosis of cancer cells measured by Annexin-FITC and CLSM. f) Cell viability of Cu(II)NS-based SDT (n = 5, mean ± SD). Scale bar: 100 μm. US: 1 MHz, 50% duty cycle, 1 W cm^{-2}, 30 s. *** indicates $p < 0.001$ according to a Student's two-tailed t-test.

Figure S8, Supporting Information, and **Figure 5**a, ^{64}Cu(II)NS exhibit a long half-life period and high tumor accumulation. In addition, serial slices of tumor from bottom to top show that ^{64}Cu(II)NS are distributed uniformly in tumor at 24 h post injection (Figure 5c). As shown in Figure 5b, with the assistance of PET/CT imaging at 72 h post injection, tumor accumulation of sonosensitizers was more clearly observed. Encouraged by the favorable performance, we calculate that the blood half-life period of ^{64}Cu(II)NS can reach 10.8 h based on the quantitative region-of-interest analysis of PET images (Figure 5d). The long half-life period endows ^{64}Cu(II)NS with the ability to steadily enter into tumor for more than 24 h (Figure S9, Supporting Information, and Figure 5e). Ex vivo biodistribution at 72 h post injection corroborated the quantification data from PET imaging. The tumor accumulation rate of ^{64}Cu(II)NS was 12.4% ID g^{-1} at 72 h post injection (Figure 5f,g). Our data show that Cu(II)NS has a long circulation period and high tumor accumulation that complement SDT.

The biological compatibility of Cu(II)NS at tested concentrations was validated prior to in vivo experiments. As shown in Figures S10 and S11, Supporting Information, Cu(II)NS presented little damage to main organs of interest, indicating good biocompatibility. After injection Cu(II)NS into the tail

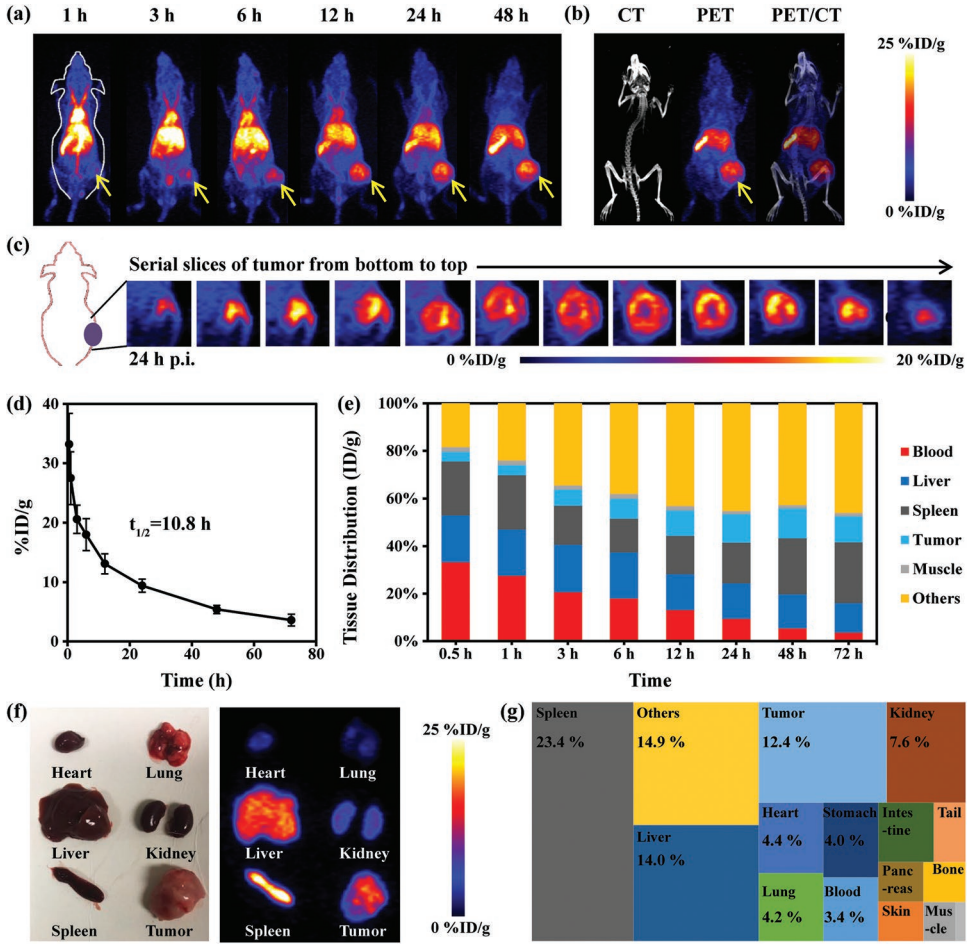

Figure 5. In vivo experiments based on 4T1-tumor-bearing mice. a) PET imaging at different time points after injection with ^{64}Cu(II)NS via tail vein. b) PET/CT imaging 72 h after injection with ^{64}Cu(II)NS and c) serial slices of tumor from bottom to top. d) Blood half-life of ^{64}Cu(II)NS (n = 3, mean ± SD). e) Tissue distribution of ^{64}Cu(II)NS at different time points after injection. f) Ex vivo PET imaging of heart, liver, spleen, lung, kidney, and tumor at 72 h after injection with ^{64}Cu(II)NS. g) Tissue distribution of ^{64}Cu(II)NS (ID g^{-1}) at 72 h after injection.

vein, the fluorescence intensity in tumor increased over time (**Figure 6**a,b). As proved above, Cu(I)NS can emit fluorescence but Cu(II)NS cannot. Although tumor contains fewer nanomaterials than liver as provided by PET imaging in Figure 5f, the fluorescence of tumor is much stronger than that of tumor in Figure 6b. In addition, the tumor has much less nanomaterials than that in the spleen as indicated by PET imaging, which provide the baseline for the accumulation of nanomaterials, but the fluorescence in tumor is enhanced to a similar level in the spleen. These data show that the overexpressed GSH in tumor will enhance the conversion of Cu(II)NS to Cu(I)NS, which recovers the fluorescence in tumor. As shown in Figure 6c, after injection of Cu(II)NS, the fluorescence of the Cu(I)NS in tumor tissues could be clearly detected by confocal imaging, further demonstrating the conversion of Cu(II)NS to Cu(I)NS in the tumor. In vivo SDT experiments were then conducted in tumor-bearing mice. As shown in Figure 6d, the weights of mice are similar across groups. The tumor growth curve (Figure 6e and Figure S12, Supporting Information) shows that the relative tumor volume at the 14th day is decreased from 17.3 ± 2.9 in control group to 2.8 ± 1.2 in Cu(II)NS+US treated group, indicating the successful tumor inhibition by the designed sonosensitizer. This therapeutic result is further confirmed by H&E staining of tumor sections (Figure 6f), which shows the damaged nuclei and cytoplasm of cancer cells in Cu(II)NS+US group, while the tumors of other groups still keep integral cell structures. Our data show that the TME-triggered Cu(II)NS has potential for therapeutic applications.

4. Conclusion

We have developed a novel open-shell nanosensitizer Cu(II)NS for cancer SDT and a detailed mechanism of GSH-responsive SDT was presented. The lack of a S_0 state due to the open-shell structure of Cu(II)NS results in little sonosensitivity. Cu(II)NS is reduced from interactions with overexpressed GSH in TME, leading to recuperative sonosensitivity of the generated Cu(I)NS. Our data show that GSH-mediated Cu(II)NS can undoubtedly increase the tumor selectivity of SDT. In addition, the long circulation period of Cu(II)NS increases the accumulation in

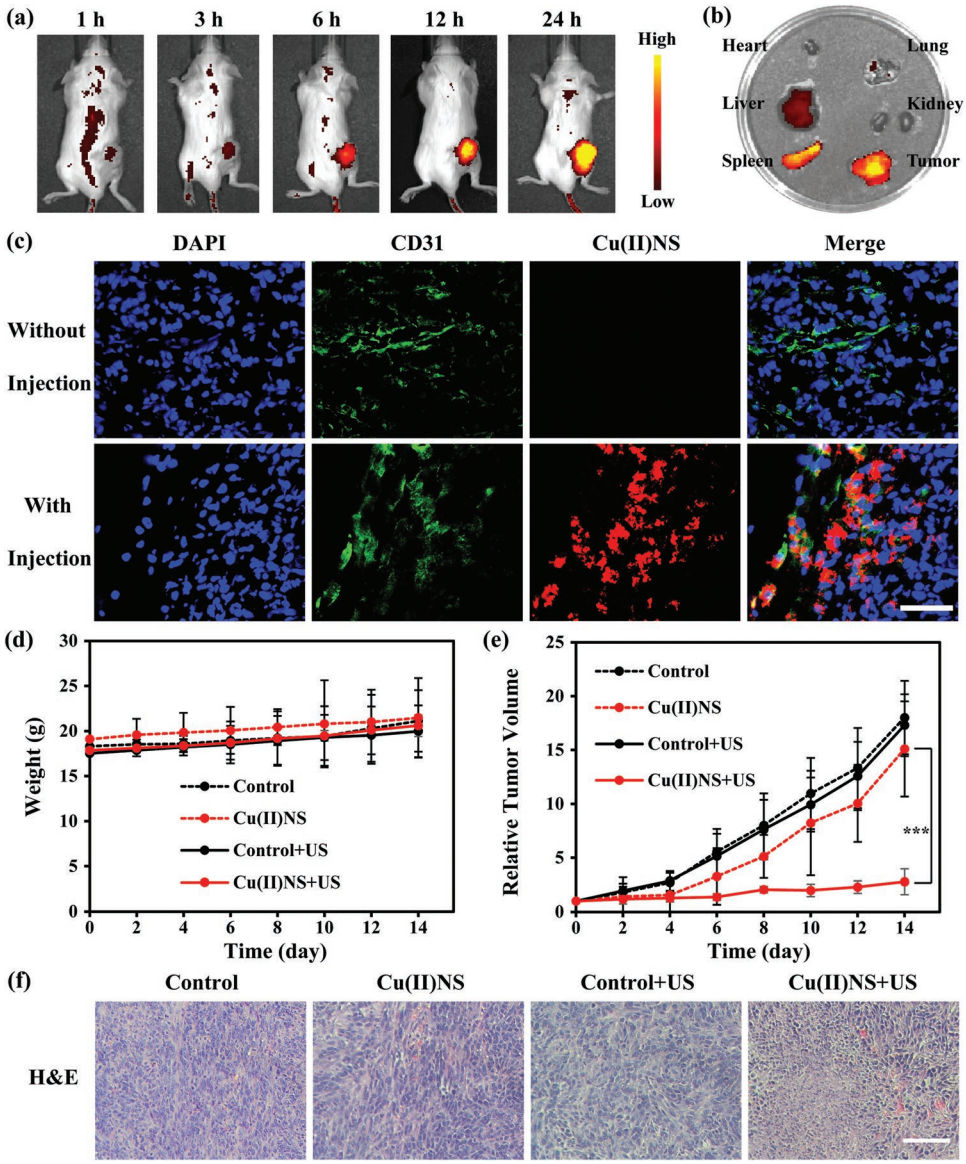

Figure 6. In vivo experiments. a) Fluorescence imaging of 4T1-tumor-bearing mice at different time points after injection with Cu(II)NS via tail vein. b) Fluorescence imaging of the heart, liver, spleen, lung, kidney, and tumor at 24 h after injection. c) Confocal imaging of tumor sections after staining with DAPI and CD31 (tumor vessels) with or without injection with Cu(II)NS. d) Body weight and e) relative tumor volume of each group ($n = 5$, mean ± SD, *** indicates $p < 0.001$ according to a Student's two-tailed t-test). f) H&E staining of tumor sections of each group. Scale bar: 50 µm. US: 1 MHz, 50% duty cycle, 2 W cm^{-2}, 120 s.

tumor to further enhance the effect of SDT. By regulating the valence state of Cu, we acquire a new kind of bioresponsive nanosensitizers and achieve cancer SDT with enhanced therapeutic index. Additionally, there are still some outstanding questions in the field of SDT such as the mechanism of sonoluminescence and the bio-effect of US. We hope that more studies will be carried out to solve these problems in the future.

Supporting Information

Supporting Information is available from the Wiley Online Library or from the author.

Acknowledgements

H.W. and J.G. contributed equally to this work. The authors acknowledge the financial support from National Natural Science Foundation of China (Grant Nos. 82102190 and 62173223), the fellowship of China Postdoctoral Science Foundation (Grant No. 2020M681326), Shanghai Municipal Education Commission—Gaofeng Clinical Medicine Grant Support (Grant No. 20191805), Foundation of National Facility for Translational Medicine (Shanghai) (Grant No. TMSK-2021-122), University of Wisconsin-Madison, the National Institutes of Health (P30CA014520), and the experiment condition of the National Facility for Translational Medicine (Shanghai).

Conflict of Interest

W.C. is a scientific advisor, stockholder, and grantee of Focus-X Therapeutics, Inc. All other authors declare no conflict of interest.

Data Availability Statement

The data that support the findings of this study are available from the corresponding author upon reasonable request.

Keywords

glutathione response, nanomedicine, open shell, positron emission tomography imaging, sonodynamic therapy

Received: December 16, 2021
Revised: February 13, 2022
Published online: March 7, 2022

[1] a) P. Zhu, Y. Chen, J. Shi, *Adv. Mater.* **2020**, *32*, 2001976; b) Y. Liu, Y. Wang, W. Zhen, Y. Wang, S. Zhang, Y. Zhao, S. Song, Z. Wu, H. Zhang, *Biomaterials* **2020**, *251*, 120075; c) F. Gong, L. Cheng, N. Yang, Y. Gong, Y. Ni, S. Bai, X. Wang, M. Chen, Q. Chen, Z. Liu, *Nat. Commun.* **2020**, *11*, 3712; d) Y. Dong, S. Dong, B. Liu, C. Yu, J. Liu, D. Yang, P. Yang, J. Lin, *Adv. Mater.* **2021**, *33*, 2106838; e) S. Liang, X. Xiao, L. Bai, B. Liu, M. Yuan, P. Ma, M. Pang, Z. Cheng, J. Lin, *Adv. Mater.* **2021**, *33*, 2100333.

[2] S. Liang, X. Deng, P. Ma, Z. Cheng, J. Lin, *Adv. Mater.* **2020**, *32*, 2003214.

[3] L. Gu, D. J. Mooney, *Nat. Rev. Cancer* **2016**, *16*, 56.

[4] a) D. F. Quail, J. A. Joyce, *Nat. Med.* **2013**, *19*, 1423; b) Z. Tang, Y. Liu, M. He, W. Bu, *Angew. Chem., Int. Ed.* **2019**, *58*, 946; c) X. Liu, Y. Li, K. Wang, Y. Chen, M. Shi, X. Zhang, W. Pan, N. Li, B. Tang, *Nano Lett.* **2021**, *21*, 7862; d) W. Zhang, J. Lu, X. Gao, P. Li, W. Zhang, Y. Ma, H. Wang, B. Tang, *Angew. Chem., Int. Ed.* **2018**, *57*, 4891.

[5] D. Ni, D. Jiang, H. F. Valdovinos, E. B. Ehlerding, B. Yu, T. E. Barnhart, P. Huang, W. Cai, *Nano Lett.* **2017**, *17*, 3282.

[6] a) S. Kim, J. W. Ginsbach, J. Y. Lee, R. L. Peterson, J. J. Liu, M. A. Siegler, A. A. Sarjeant, E. I. Solomon, K. D. Karlin, *J. Am. Chem. Soc.* **2015**, *137*, 2867; b) W. W. Su, H. Wang, T. Wang, X. Li, Z. M. Tang, S. Zhao, M. Zhang, D. N. Li, X. W. Jiang, T. Gong, W. Yang, C. J. Zuo, Y. L. Wu, W. B. Bu, *Adv. Sci.* **2020**, *7*, 1903585; c) D. Ni, D. Jiang, C. J. Kutyreff, J. Lai, Y. Yan, T. E. Barnhart, B. Yu, H.-J. Im, L. Kang, S. Y. Cho, Z. Liu, P. Huang, J. W. Engle, W. Cai, *Nat. Commun.* **2018**, *9*, 5421; d) H. Wang, B. Lv, Z. M. Tang, M. Zhang, W. Q. Ge, Y. Y. Liu, X. H. He, K. L. Zhao, X. P. Zheng, M. Y. He, W. B. Bu, *Nano Lett.* **2018**, *18*, 5768.

[7] a) B. Yu, D. Ni, Z. T. Rosenkrans, T. E. Barnhart, H. Wei, C. A. Ferreira, X. Lan, J. W. Engle, Q. He, F. Yu, W. Cai, *Adv. Mater.* **2019**, *31*, 1904894; b) B. Yu, H. Wei, Q. He, C. A. Ferreira, C. J. Kutyreff, D. Ni, Z. T. Rosenkrans, L. Cheng, F. Yu, J. W. Engle, X. Lan, W. Cai, *Angew. Chem., Int. Ed.* **2018**, *57*, 218; c) D. Ni, C. A. Ferreira, T. E. Barnhart, V. Quach, B. Yu, D. Jiang, W. Wei, H. Liu, J. W. Engle, P. Hu, W. Cai, *J. Am. Chem. Soc.* **2018**, *140*, 14971.

[8] a) G. Feng, G.-Q. Zhang, D. Ding, *Chem. Soc. Rev.* **2020**, *49*, 8179; b) C. Chen, H. Ou, R. Liu, D. Ding, *Adv. Mater.* **2020**, *32*, 1806331.

[9] a) Q. Yao, J. Fan, S. Long, X. Zhao, H. Li, J. Du, K. Shao, X. Peng, *Chem* **2021**, *8*, 197; b) S. S. Lucky, K. C. Soo, Y. Zhang, *Chem. Rev.* **2015**, *115*, 1990; c) W. Fan, P. Huang, X. Chen, *Chem. Soc. Rev.* **2016**, *45*, 6488.

[10] L. Wang, S. Duan, P. Jin, H. She, J. Huang, Z. Lei, T. Zhang, Q. Wang, *Appl. Catal., B* **2018**, *239*, 599.

[11] D. Chen, Z. Hao, X. Zhao, Z. Wang, *J. Mol. Struct.: THEOCHEM* **2007**, *803*, 73.

[12] a) B. Krasovitski, V. Frenkel, S. Shoham, E. Kimmel, *Proc. Natl. Acad. Sci. USA* **2011**, *108*, 3258; b) A. Azagury, E. Amar-Lewis, Y. Yudilevitch, C. Isaacson, B. Laster, J. Kost, *Ultrasound Med. Biol.* **2016**, *42*, 1560.